Chinese Journal of Chemical Engineering 55 (2023) 84–92

Contents lists available at ScienceDirect

Chinese Journal of Chemical Engineering

journal homepage: www.elsevier.com/locate/CJChE

Full Length Article

Different efficiency toward the biomimetic aerobic oxidation of benzyl alcohol in microchannel and bubble column reactors: Hydrodynamic characteristics and gas–liquid mass transfer

Qi Han [1], Xin-Yuan Zhang [1], Hai-Bo Wu [3], Xian-Tai Zhou [1,3,*], Hong-Bing Ji [2,*]

[1] Fine Chemical Industry Research Institute, School of Chemical Engineering and Technology, Sun Yat-sen University, Zhuhai 519082, China
[2] Fine Chemical Industry Research Institute, School of Chemistry, Sun Yat-sen University, Guangzhou 510275, China
[3] Huizhou Research Institute, Sun Yat-sen University, Huizhou 516081, China

ARTICLE INFO

Article history:
Received 7 March 2022
Received in revised form 14 May 2022
Accepted 16 May 2022
Available online 13 June 2022

Keywords:
Membrane microchannel reactor
Gas–liquid flow
Mass transfer
Benzyl alcohol
Computational fluid dynamics (CFD)
Bubble column reactor

ABSTRACT

The selective aerobic oxidation of benzyl alcohol to benzaldehyde has attracted considerable attention because benzaldehyde is a high value-added product. The rate of this typical gas–liquid reaction is significantly affected by mass transfer. In this study, CoTPP-mediated (CoTPP: cobalt (II) *meso*-tetraphenylporphyrin) selective benzyl alcohol oxidation with oxygen was conducted in a membrane microchannel (MMC) reactor and a bubble column (BC) reactor, respectively. We observed that 83% benzyl alcohol was converted within 6.5 min in the MMC reactor, but only less than 10% benzyl alcohol was converted in the BC reactor. Hydrodynamic characteristics and gas–liquid mass transfer performances were compared for the MMC and BC reactors. The MMC reactor was assumed to be a plug flow reactor, and the dimensionless variance was 0.29. Compared to the BC reactor, the gas–liquid mass transfer was intensified significantly in MMC reactor. It could be ascribed to the high gas holdup (2.9 times higher than that of BC reactor), liquid film mass transfer coefficient (8.2 times higher than that of BC reactor), and mass transfer coefficient per unit interfacial area (3.8 times higher than that of BC reactor). Moreover, the Hatta number for the MMC reactor reached up to 0.61, which was about 15 times higher than that of the BC reactor. The computational fluid dynamics calculations for mass fractions in both liquid and gas phases were consistent with the experimental data.

1. Introduction

As benzaldehyde is widely used in organic synthesis, detection reagents, and fragrances, the selective oxidation of benzyl alcohol to benzaldehyde is an essential chemical process [1–7]. Some stoichiometric oxidants such as *tert*-butyl hydroperoxide (TBHP) [8,9], hydrogen peroxide [10–12], and nitric acid [13–16] have been used in the selective oxidation of benzyl alcohol to benzaldehyde. From the perspective of economy and environment, using molecular oxygen as oxidant is the most desirable oxidant oxidation routine [17–21]. Hence, various catalytic systems combining cobalt [22,23], manganese [24,25], ruthenium [26–28], *etc.* have been developed for the efficient benzyl alcohol oxidation.

For a typical gas–liquid reaction, most selective aerobic oxidations of benzyl alcohol are conducted in a bubble column (BC) reactor [29–31]. The disadvantages of the BC reactor are high gas phase consumption and uneven gas–liquid contacting [32–33]. Therefore, the enhancement of gas–liquid mass transfer is a significant strategy to improve efficiency for benzyl alcohol oxidation [34].

Recently, microchannel technology has been developed rapidly and was gained attention in biological and chemical industries. The permeable membrane microchannel (MMC) reactors were designed and used in various catalytic reactions [35–37]. Various reactions such as partial oxidation of methane and oxidative coupling of methane [38–40], nitration [41], epoxidation [42,43], and peroxidation [44] can be conducted in the MMC reactor with excellent conversion and selectivity. Most recently, we reported the mechanism and kinetics studies for selective aerobic oxidation of benzyl alcohol in the MMC reactor [45]. Although the oxidation of benzyl alcohol could be converted efficiently in the MMC

* Corresponding authors.
E-mail addresses: zhouxtai@mail.sysu.edu.cn (X.-T. Zhou), jihb@mail.sysu.edu.cn (H.-B. Ji).

https://doi.org/10.1016/j.cjche.2022.05.020
1004-9541/

reactor, studies on the mass transfer enhancement performance and hydrodynamic characteristics are still limited.

In this research, the aim was to study the hydrodynamic characteristics and gas–liquid mass transfer performances for both MMC and BC reactors. For comparison, the mass transfer parameters such as gas holdup, liquid film mass transfer coefficient, and mass transfer coefficient per unit interfacial area were measured towards the selective aerobic oxidation of benzyl alcohol catalyzed by cobalt porphyrin. In addition, the ratio of the reaction rate to the mass transfer rate (Hatta number) was determined for each reactor. CFD calculations for mass fractions in both liquid and gas phases were carried out to prove that they were consistent with the experimental data. This study may provide a much deeper understanding of the hydrodynamic characteristics and gas–liquid mass transfer in a microchannel reactor.

2. Experimental

2.1. Catalytic performance

In BC reactor, the liquid phase contained benzyl alcohol, 1,2-dichloroethane and the catalyst was mixed in the bubble column. Dioxygen was bubbled from the gas inlet at the bottom of the column. The products generation and benzyl alcohol consuming were measured by GC (Shimadzu GC-2010 Plus) equipped with a Rtx-5 capillary column (30 m × 0.25 mm × 0.25 mm).

In MMC reactor, isobutyraldehyde dissolved in 1,2-dichloroethane was pumped by a plunger pump at 4 ml·min^{-1} flow rate (Fluid X). Another solution containing benzyl alcohol, 1,2-dichloroethane and CoTPP catalyst was pumped by a plunger pump at 4 ml·min^{-1} flow rate (Fluid Y). Fluids X and Y were mixed in a T-mixer. Then, the liquid phases were delivered into the MMC reactor to contacted with gas phase. The reaction was carried out in an isothermal system heating by an air heat exchanger (Fig. 1). The products generation and benzyl alcohol consuming were measured by GC equipped with a Rtx-5 capillary column.

2.2. Residence time distribution

Procedures for the aerobic oxidation of benzyl alcohol in MMC and BC reactor were described in Supporting Information. Residence time distribution (RTD) measurements were conducted in the MMC reactor by the tracer method [46]. A solution of naphthalene in DCE (1,2-dichloroethane, 0.005 mol·L^{-1}) was used as a tracer, and its concentration was measured by GC. Moreover, the residence time distribution function, $F(t)$, and the residence time distribution density function, $E(t)$, were calculated using Eqs. (1) and (2), respectively.

$$F(t)=\frac{N_t}{N_\infty}=\frac{\int_0^t V_t\mathrm{d}t}{\int_0^\infty V_t\mathrm{d}t}=\int_0^t\frac{V_t}{m_\infty}\mathrm{d}t=\frac{\sum_0^t c_{\text{naphthalene}}}{\sum_0^\infty c_{\text{naphthalene}}} \tag{1}$$

$$E(t)=\frac{\mathrm{d}F(t)}{\mathrm{d}t}=\frac{V_t}{m_\infty}=\frac{c_{\text{naphthalene}}}{\Delta t\sum_0^\infty c_{\text{naphthalene}}} \tag{2}$$

2.3. Gas−liquid mass transfer

The gas holdup of oxygen was measured in a thin glass tube with 1.2 cm diameter. The solution for catalytic oxidation was introduced in the glass tube and then, oxygen was fed at 65 °C for 500 s. The liquid levels before (h_l) and after (h_{l+g}) bubbling oxygen (Fig. S1 in Supplementary Material) were measured to calculate gas holdup using Eq. (3).

$$\varepsilon=\frac{h_{l+g}-h_l}{h_{l+g}} \tag{3}$$

The relevant parameters of liquid-film mass transfer were investigated by conducting experiments and calculated using Eqs. (4)–(6). The accuracy and derivation process of these formulas was confirmed (Supplementary Material). The flow velocity of the solution flowing into and out of the reactor was measured by a rotameter. The oxygen concentration was measured by dissolved oxygen meters [47–50].

$$N_O=k_La\cdot(C_O{}^*-C_O)=\frac{v_1-v_2}{V} \tag{4}$$

$$K_L=\frac{k_La}{A} \tag{5}$$

$$\gamma=\frac{\sqrt{k_{A-B}D_Ac_B}}{K_L} \tag{6}$$

All mass transfer parameters were reproducible within an experimental error of ±5%.

2.4. CFD modeling

The simulation of conversion, selectivity and gas holdup were performed in isothermal steady system by a commercial CFD software package ANSYS® Fluent on a Hasee Notebook Z7M (i5 Intel hexa-core and hexa-thread processors, Pro Win10 Professional® x64, available RAM 32.0 GB and ROM 1.0 T). The gird meshed with prismatic and hexahedral elements including a total of 80,210 volume elements. In addition, the grid independence was demonstrated through the gas holdup simulations. The axial variations of gas holdup in MMC reactor (liquid flow: 6 ml·min^{-1}) with different grid number as shown in Fig. S2. It showed that the grid is independent of grid number when its value was higher than 80210.

The geometry modeling of the microchannel reactor and the bubble column reactor was a pipe-in-pipe structure, as shown in Figs. S3 and S4. We simplified the gas phase in the microchannel reactor; the gas was introduced as tiny bubbles and allowed to permeate radially in the liquid phase from the gas inlet on the semipermeable membrane (Fig. S3). The microchannel diameter and range were 2 mm and 0.5 m, respectively. The liquid flow velocity was 0.02 m·s^{-1}, and the gas flow velocity was 0.02 m·s^{-1}. The diameter of the bubbles in the liquid phase was 0.01 mm. The bubble column was simulated as a cylinder with a basal diameter of 60 mm and a height of 140 mm (Fig. S4).

At the bottom of the cylinder, there was a gas inlet with 2.5 mm diameter and at the top, there was a gas outlet. The gas flow velocity was 0.02 m·s^{-1}, and the bubble diameter was 2 mm. The Eulerian−Eulerian multiphase flow model, which is suitable for a multiphase mixing model and allows interphase mass transfer, was used in the simulation. Eqs. (7)–(10) represent the mass, species and momentum transport equations, respectively. Gas−liquid mass transfer was defined by Henry's law. The chemical reaction model used was based on FEM. The activation energy of biomimetic aerobic oxidation of benzyl alcohol was 70.3 kJ·mol^{-1}.

Continuity equations:

$$\text{gas phase}:\ \frac{\partial}{\partial t}\left(\alpha_g\rho_g\right)+\nabla\cdot\left(\alpha_g\rho_gu_g\right)=0 \tag{7}$$

$$\text{liquid phase}:\ \frac{\partial}{\partial t}(\alpha_l\rho_l)+\nabla\cdot(\alpha_l\rho_lu_l)=0 \tag{8}$$

Momentum equations:

$$\text{gas phase}: \frac{\partial(\alpha_g\rho_g u_g)}{\partial t}+\nabla\cdot\left(\alpha_g\rho_g u_g u_g\right)=\nabla\cdot\left(\alpha_g\tau_g\right)-\alpha_g\nabla p+\alpha_g\rho_g g-M_{l,g} \quad (9)$$

$$\text{liquid phase}: \frac{\partial(\alpha_l\rho_l u_l)}{\partial t}+\nabla\cdot(\alpha_l\rho_l u_l u_l)=\nabla\cdot(\alpha_l\tau_l)-\alpha_l\nabla p+\alpha_l\rho_l g-M_{l,g} \quad (10)$$

Since a reaction can change with the reaction time, a transient solver was used throughout the simulation. In addition, the liquid flow in the microchannel was laminar flow because the Reynolds number was less than 1.0. Environmental conditions: no gravity, atmospheric pressure, and 65 °C temperature. Flow conditions: benzyl alcohol (10% mass fraction), activation energy (E_a, 70.3 kJ·mol^{-1}), liquid flow velocity (0.02 m·s^{-1}), and gas flow velocity (0.02 m·s^{-1}). The phase coupled simple algorithm and first order upwind were used to discretize and solve the two-phase mass transfer equation.

3. Results and Discussion

3.1. Catalytic aerobic oxidation of benzyl alcohol in MMC and BC reactors

Aerobic oxidation of benzyl alcohol was conducted in MMC and BC reactors (Fig. 2). In the MMC reactor, the conversion of benzyl alcohol reached up to 83% within 6.5 min; however, only less than 10% conversion was obtained in the BC reactor at the same reaction time (Fig. 2(a)). Even when the reaction time was prolonged to 30 min, the conversion of benzyl alcohol was only 64% in the BC reactor. It showed that the reaction rate of benzyl alcohol oxidation increased significantly in the MMC reactor.

In addition to catalytic efficiency, the selectivity towards benzaldehyde increased considerably in the MMC reactor (Fig. 2(b)). In the BC reactor, the selectivity to benzaldehyde and benzoic acid were almost equal (about 50%). This indicated consecutive oxidation reactions (benzyl alcohol to benzaldehyde and benzaldehyde

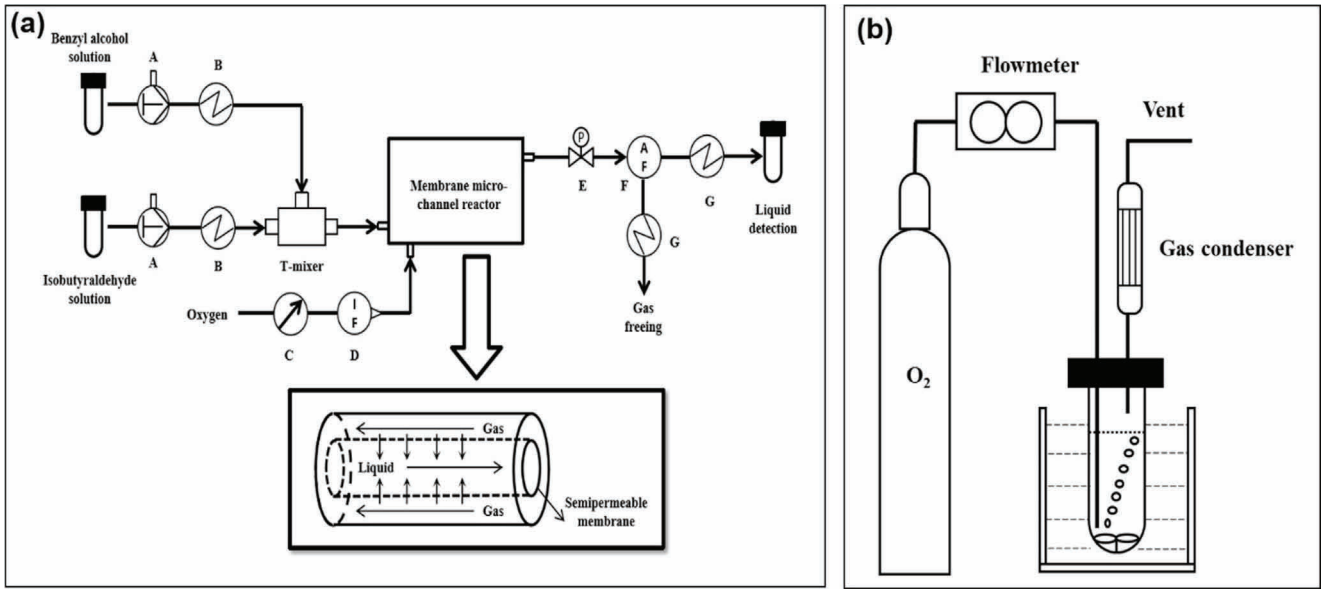

Fig. 1. Schematic diagrams of reactor: (a) the membrane microchannel (A: pump, B: preheater, C: gas pressure gauge, D: mass-flow controller, E: back pressure valve, F: gas–liquid separator, G: condenser); (b) the bubble column.

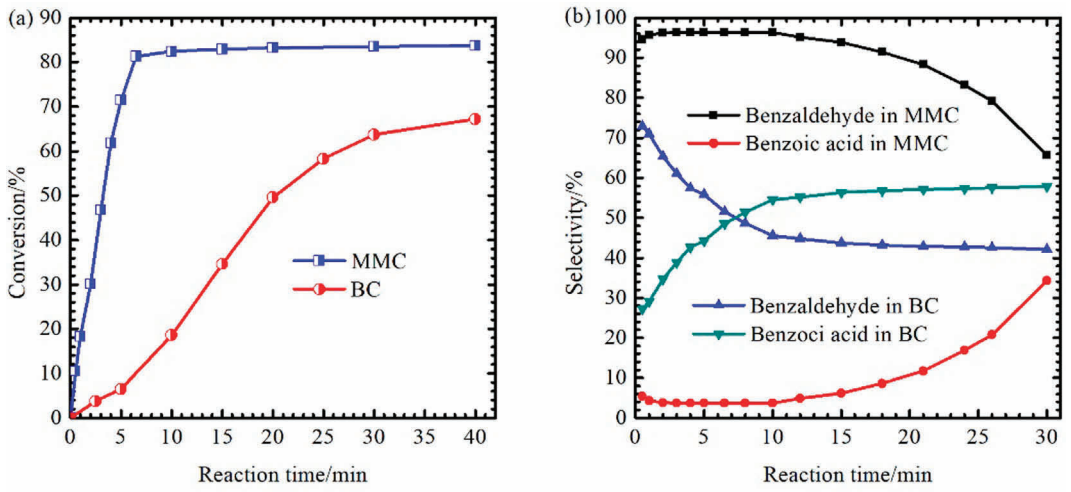

Fig. 2. Aerobic oxidation of benzyl alcohol catalyzed by CoTPP in the presence of isobutyraldehyde in MMC and BC reactors: (a) benzyl alcohol conversion; (b) selectivity towards benzaldehyde and benzoic acid. Benzyl alcohol (0.23 mol·L^{-1}), isobutyraldehyde (0.92 mol·L^{-1}), CoTPP (1.80 × 10^{-4} mol·L^{-1}), liquid flow (4.0 ml·min^{-1}), air flow (15 ml·min^{-1}), and 65 °C.

to benzoic acid). However, the selectivity to the two products were quite different in the MMC reactor, in which 96% selectivity to benzaldehyde was obtained within 6.5 min. In addition, when the reaction time was prolonged in the MMC reactor, the oxidation of benzaldehyde to benzoic acid was observed. From the observed results, it could be inferred that the reaction rates for consecutive oxidation reactions tended to be approximately equal. The high selectivity of benzaldehyde in MMC reactor could be attributed to the short residence time and excellent concentration distribution. Hence, the enhancement of gas–liquid mass transfer is favorable for the formation of benzaldehyde in a short reaction time.

3.2. Hydrodynamics of reactors

The residence time distribution of the liquid phase in a reactor is a significant operating parameter for mass transfer, which and it can affect the efficiency and selectivity of the products. The concentration of the tracer in terms of output was used for the estimation of mean residence time and variance.

The residence time distribution function, $F(t)$, and the residence time distribution density function, $E(t)$, were calculated using Eqs. (1) and (2), respectively. Typical $F(t)$ and $E(t)$ curves for the MMC reactor under the reaction conditions are shown in Fig. 3. The comparison between the experimental curve and the theoretical models indicated that the experimental data were well represented. The mean residence time for benzyl alcohol oxidation in the MMC reactor was 238.32 s; the variance was 16483.78 s^2, and the dimensionless variance was 0.29. This indicated that the hydrodynamics of the MMC reactor tended to be those of a plug flow reactor (PFR). For the bubble column reactor, the residence time of the tracer was the same as that of the reactants under the reaction conditions. Hence, the hydrodynamics of the BC reactor tended to be those of a continuous stirred-tank reactor (CSTR).

In addition, the material balance of benzyl alcohol in the MMC reactor was calculated, as shown in Table S1. It was worth noting that there was only 4.14%–5.22% benzyl alcohol retention. Due to the plug flow-like characteristics of MMC reactor, the gas and liquid fluids involved in the reaction were pumped to flow at a set rate. Therefore, there was no dead volume in the MMC reactor. The benzyl alcohol retention could be attributed to the dead volume of the T-mixer.

3.3. Gas–liquid mass transfer

The gas holdup (ε) of oxygen is an important parameter to determine different flow regimes in a gas–liquid reactor. According to the calculations obtained using Eq. (3), the variation trends of gas holdup with air flow for MMC and BC reactors are shown in Fig. 4(a). The gas holdup increased with the increase in air flow in both MMC and BC reactors. However, it was clear that at the same air flow, the gas holdup in the MMC reactor was considerably higher than that in the BC reactor. For the MMC reactor, the gas holdup reached 80% at 30 ml·min^{-1} air flow, and it could be maintained when the air flow increased continuously. For the BC reactor, the maximum gas holdup was only about 28%. This indicated that the gas could not be easily dispersed into the liquid phase in the BC reactor.

The liquid film mass transfer coefficient (k_La) is the coefficient used to calculate the mass transfer rate according to the driving force and resistance of the liquid film alone in a gas–liquid mass transfer system [45]. It was calculated using Eq. (4), and the relevant typical parameters are listed in Tables S2 and S3. It was observed that the k_La value increased with the increase in air flow (Fig. 4(b)), which indicated that there was continuous mass transfer between gas and liquid phase in the whole liquid film. For the air flow range of 10–30 ml·min^{-1}, the k_La value increased from 318 min^{-1} to 666 min^{-1} for the MMC reactor. However, the increase in the k_La value in the same range for the BC reactor was much lower than that observed for the MMC reactor (12–81 min^{-1}). This indicated that oxygen diffused completely in the liquid film in the MMC reactor.

The calculations of the gas–liquid interfacial area (A), bubble size (d_b), and mass transfer coefficient per unit interfacial area (K_L) were carried out to compare the rates of gas–liquid mass transfer between MMC and BC reactors. Bubble diameters were calculated using Eq. (11) [51], and gas–liquid interfacial areas were calculated using Eq. (12) [51].

$$d_b = 1.82 \times \left[\frac{d_0\sigma_l}{(\rho_l - \rho_g)g}\right]^{\frac{1}{3}} \tag{11}$$

$$A = \frac{6\varepsilon}{d_b(1-\varepsilon)} \tag{12}$$

In general, the bubble size in one type of a reactor is almost uniform. As shown in Tables S4 and S5, the bubble diameters were 2.1 mm and 5.3 mm in MMC and BC reactors, respectively. The values of the gas–liquid interfacial area (7000–15000 m^{-1}) obtained for the MMC reactor were 15–20 times higher than those obtained for the BC reactor (Fig. 5(a)).

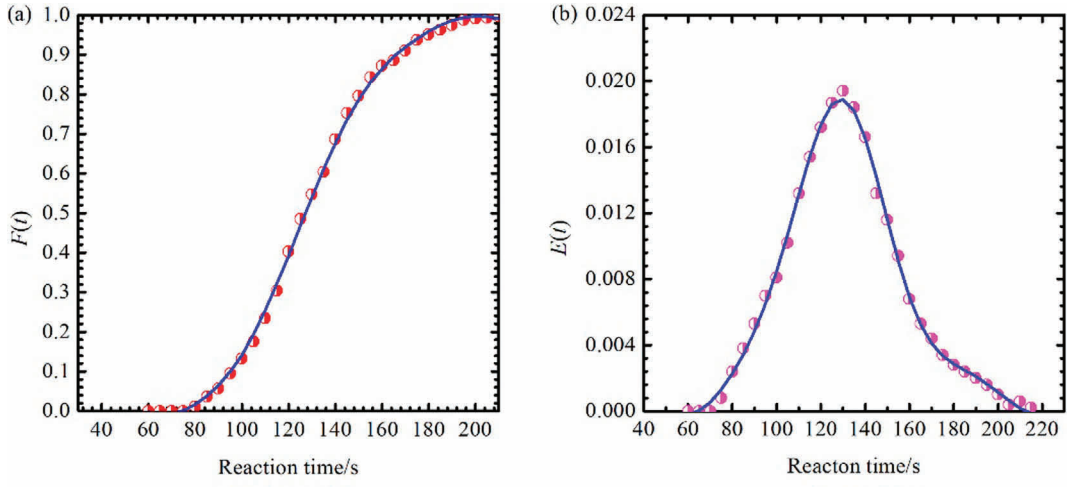

Fig. 3. (a) Residence time distribution function, $F(t)$, and (b) residence time distribution density function, $E(t)$, for the MMC reactor.

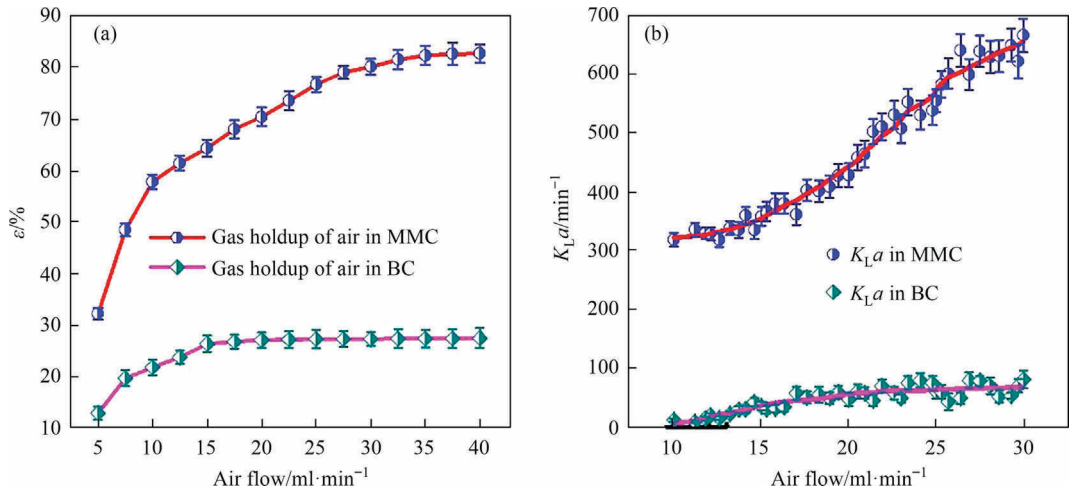

Fig. 4. Comparisons of (a) gas holdup and (b) liquid film mass transfer coefficients between MMC and BC reactors at different air flow values. Benzyl alcohol (0.23 mol·L^{-1}), isobutyraldehyde (0.92 mol·L^{-1}), CoTPP (1.80 × 10^{-4} mol·L^{-1}), liquid flow (8.0 ml·min^{-1}), and 65 °C.

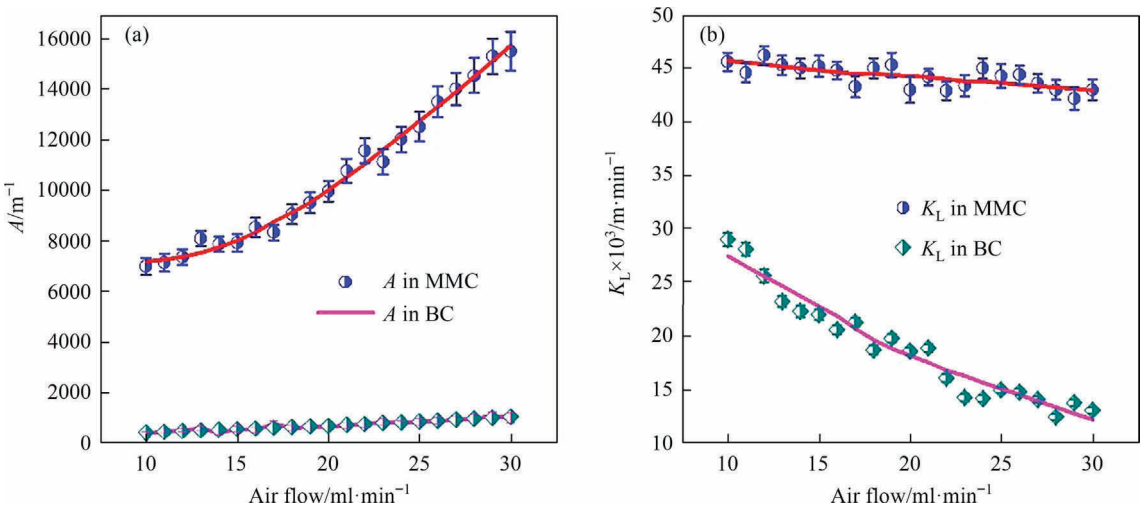

Fig. 5. Comparisons of (a) gas–liquid interfacial area and (b) mass transfer coefficient per unit interfacial area between MMC and BC reactors. Benzyl alcohol (0.23 mol·L^{-1}), isobutyraldehyde (0.92 mol·L^{-1}), CoTPP (1.80 × 10^{-4} mol·L^{-1}), liquid flow (8.0 ml·min^{-1}), and 65 °C.

The values for the mass transfer coefficient per unit interfacial area (K_L) were obtained using Eq. (5) (Fig. 5(b)). For the MMC reactor, it was observed that there were no considerable changes in the K_L values with the increase in air flow. However, for the BC reactor, the K_L values decreased gradually from 2.9 × 10^{-2} to 1.3 × 10^{-2} m·min^{-1} with the increase in the air flow from 10 to 30 ml·min^{-1}. This indicated that the oxygen utilization in the BC reactor was much lower than that in the MMC reactor. The increased oxygen in reactor resulted in the increased gas–liquid interfacial area. In BC reactor, due to the limit of gas–liquid mass transfer, the increased mass transfer coefficient was not significant with the increased air flow. While for MMC reactor, the continuous gas was dispersed in the liquid phase evenly in presence of semipermeable membrane. The mass transfer coefficient in MMC reactor increased significantly with the improved air flow.

The Hatta number (γ) is the ratio of the chemical reaction rate to the mass transfer rate. The calculations of Hatta number for benzyl alcohol oxidation in MMC and BC reactors were carried out using Eq. (6). The diffusion coefficient (D_A) was calculated using Eq. (13), in which the physical parameters of the liquid phase such as density, viscosity, and surface tension were calculated by the liquid distribution principle based on the basic data obtained from chemical industries (Tables S6 and S7).

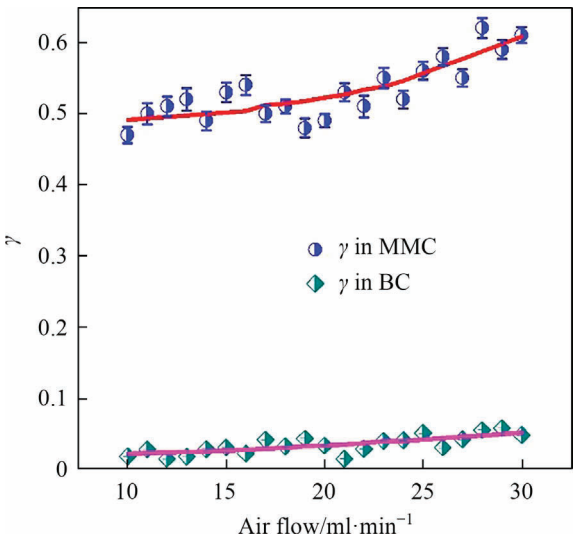

Fig. 6. Comparison of Hatta number (γ) between MMC and BC reactors. Benzyl alcohol (0.23 mol·L^{-1}), isobutyraldehyde (0.92 mol·L^{-1}), CoTPP (1.80 × 10^{-4} mol·L^{-1}), liquid flow (8.0 ml·min^{-1}), and 65 °C.

$$D_A = \frac{7.4 \times 10^{-8}(\Psi M)^{0.5} T}{\mu V_A^{0.6}} \quad (13)$$

As shown in Fig. 6, the γ value for the MMC reactor is much higher than that for the BC reactor at the air flow range from 10 to 30 ml·min^{-1}. For the MMC reactor, with the increase of air flow, the γ value was increased from 0.49 to 0.61. However, no considerable increase in the γ value was observed for the BC reactor. The reaction rate was divided into three types qualitatively according to the Hatta number (as shown in Table S8). Therefore, based on the γ values, we concluded that the aerobic oxidation of benzyl alcohol in the MMC reactor was a reaction with moderate rate [52–55].

3.4. CFD simulations

CFD simulations were carried out to distinguish the concentration distribution of benzyl alcohol and benzaldehyde for MMC and BC reactors. The corresponding simulations were conducted according to the same stoichiometric experimental conditions. Fig. 7(a) and (b) shown the three-dimensional and two-dimensional models of the mass fraction of benzyl alcohol, respectively, in the MMC reactor. It was observed that there were sufficient reaction areas for benzyl alcohol conversion to benzaldehyde provided by the long channels in the MMC reactor. Also, from the simulations of the mass fraction of benzaldehyde, shown in Fig. 7(c) and (d), it was inferred that benzaldehyde could be generated steadily with a continuous flow in the MMC reactor. Molecular oxygen was introduced into the liquid phase continuously through pressure. Hence, the diffused oxygen could be utilized completely, which was helpful to enhance the selectivity of benzaldehyde.

Fig. 8 shows the two-dimensional models of the mass fraction of benzyl alcohol and benzaldehyde in the BC reactor. It could be observed that benzyl alcohol was hardly converted due to the limited gas–liquid transfer (Fig. 8(a)), which indicated that the utilization of oxygen was extremely low. In addition, the concentration distributions of oxidized products were uneven in the reactor (Fig. 8(b)). The simulation results were consistent with the experimental results, which indicated that the utilization of oxygen was low in the BC reactor.

Moreover, the gas volume fraction in the liquid phase was calculated by means of CFD simulations under experimental conditions. As shown in Fig. 9(a), oxygen could pass through the semipermeable membrane in the MMC reactor. Oxygen was uniformly distributed in the liquid phase. Hence, high gas holdup

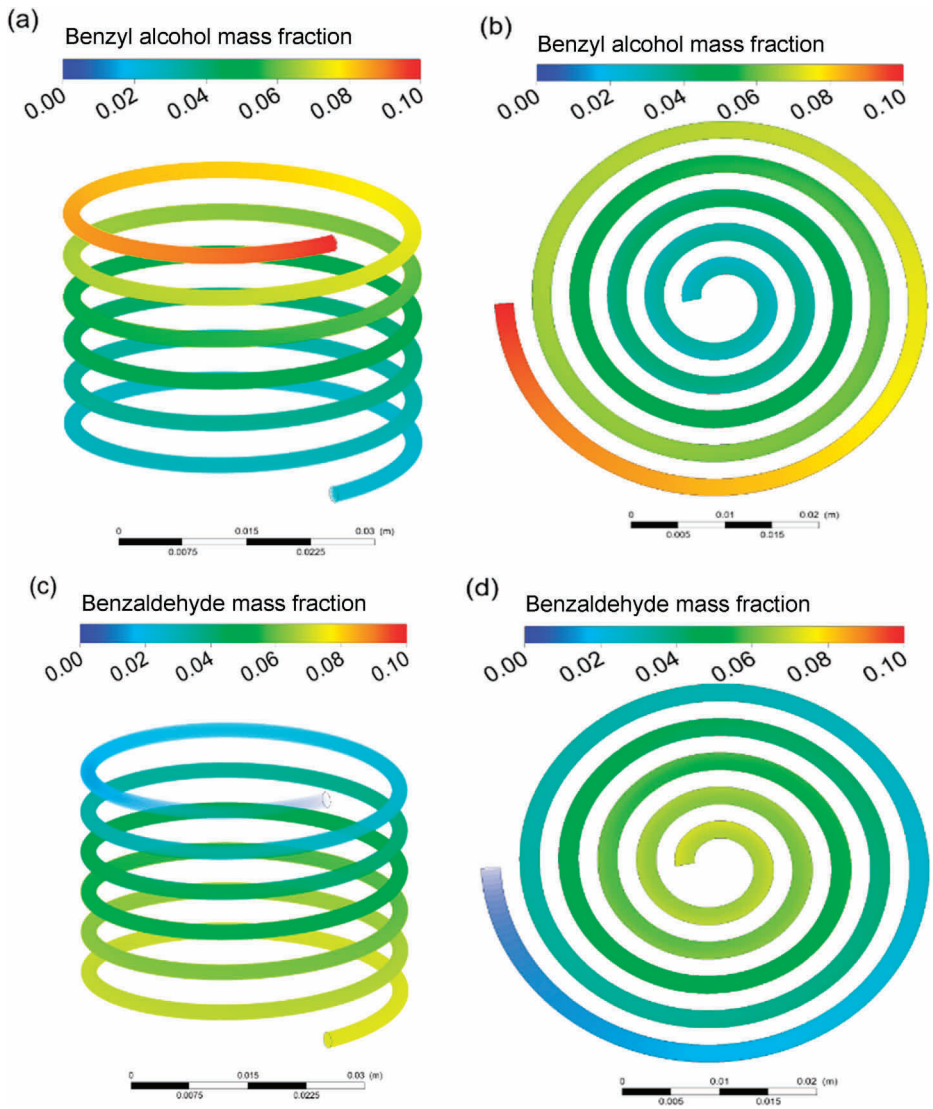

Fig. 7. Mass fractions of benzyl alcohol and benzaldehyde by CFD simulations in the MMC reactor: mass fraction of benzyl alcohol represented as (a) three-dimensional and (b) two-dimensional models; mass fraction of benzaldehyde represented as (c) three-dimensional and (d) two-dimensional models.

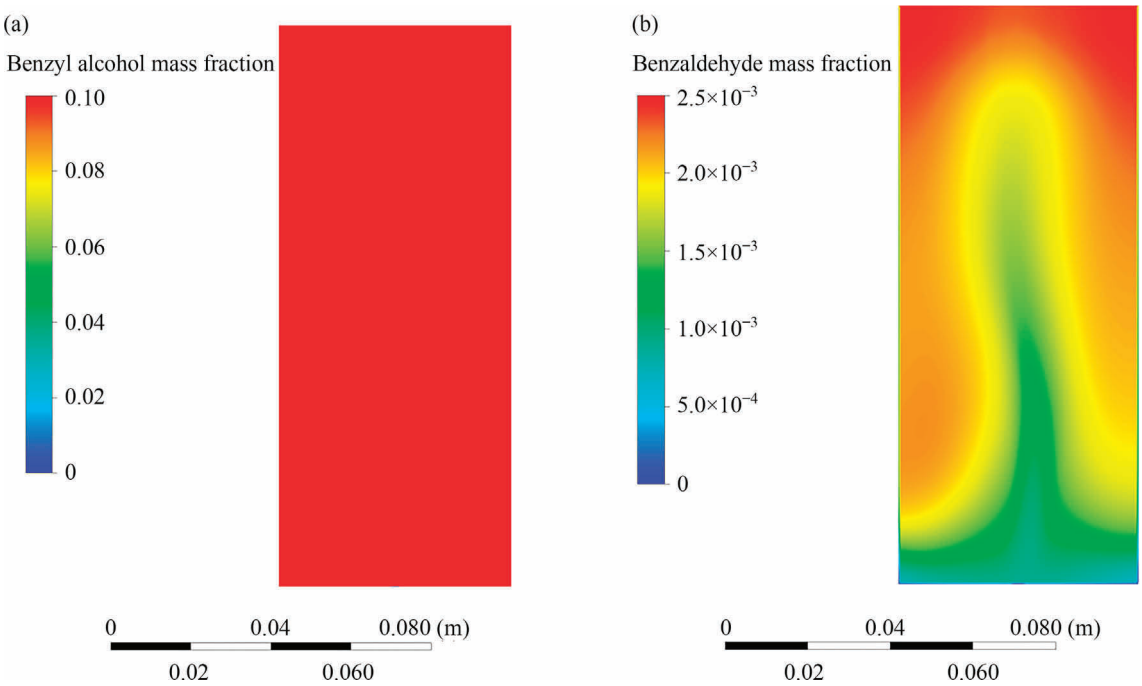

Fig. 8. Mass fractions of benzyl alcohol and benzaldehyde by CFD simulations in the BC reactor: mass fractions of (a) benzyl alcohol and (b) benzaldehyde represented as two-dimensional models.

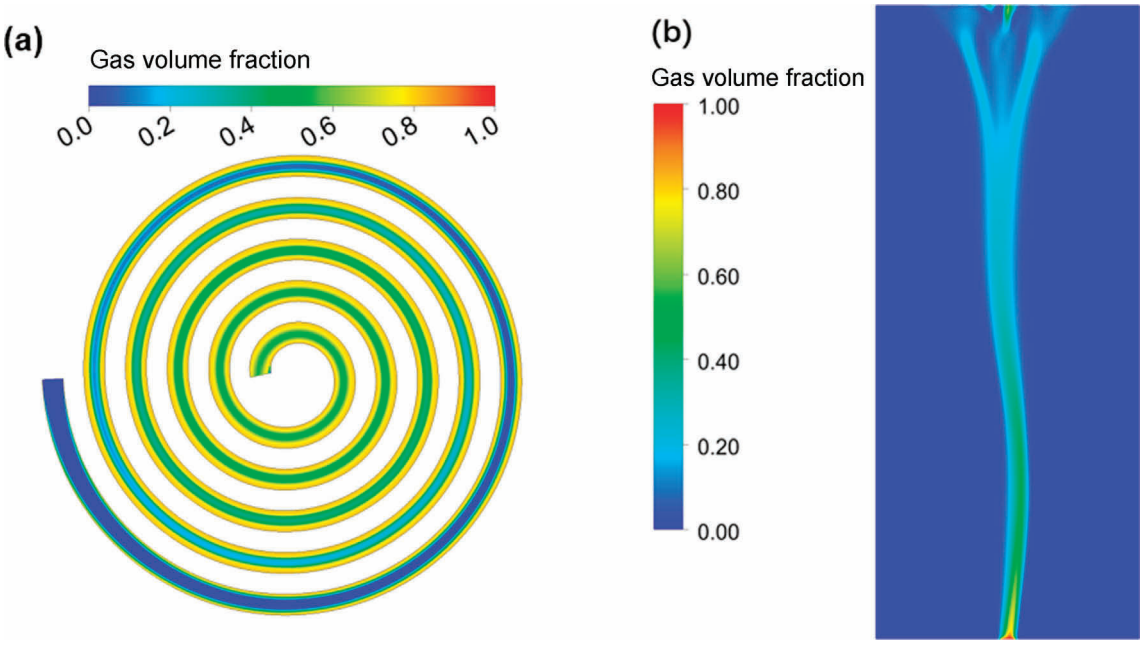

Fig. 9. Gas volume fractions in the liquid phase by CFD simulations in (a) MMC and (b) BC reactors.

(80%) could be obtained at 30 ml·min^{-1} air flow. For the BC reactor, limited by the poor gas–liquid contact surface, mixing and mass transfer proceeded only on the gas–liquid contact surface (Fig. 9 (b)). Therefore, a low gas holdup was obtained as might be expected in the BC reactor.

4. Conclusions

In summary, the significant difference in reaction rate was obtained when CoTPP-mediated selective oxidation of benzyl alcohol with oxygen was conducted in MMC and BC reactors, respectively. In the MMC reactor, the conversion of benzyl alcohol reached up to 83% within 6.5 min, and the selectivity of benzaldehyde was up to 96%. However, only 64% conversion and 45% selectivity of benzaldehyde were obtained in the BC reactor even when the reaction time was prolonged to 30 min. For comparison, the hydrodynamic characteristics and gas–liquid mass transfer performances for MMC and BC reactors were investigated. Compared to the hydrodynamics of the BC reactor, the hydrodynamics of the MMC reactor tended to be those of a plug flow reactor, and the dimensionless variance was 0.29. For the MMC reactor, the gas

holdup, liquid film mass transfer coefficient (k_La), and mass transfer coefficient per unit interfacial area (K_L) reached up to 80%, 666 min^{-1}, and 4.5×10^{-2} $m \cdot min^{-1}$ at 30 $m \cdot min^{-1}$ air flow, respectively. The Hatta number for the MMC reactor was 0.61, which was about 15 times higher than that of the BC reactor. The experimental data were consistent with the CFD calculations of mass fractions in both liquid and gas phases.

Declaration of Competing Interest

The authors declare that they have no known competing financial interests or personal relationships that could have appeared to influence the work reported in this paper.

Acknowledgements

This work was financially supported by the National Key Research and Development Program of China (2020YFA0210900), the National Natural Science Foundation of China (21938001 and 21878344), Guangdong Provincial Key Research and Development Programme (2019B110206002), the Local Innovative and Research Teams Project of Guangdong Pearl River Talents Program (2017BT01C102).

Supplementary Material

Supplementary data to this article can be found online at https://doi.org/10.1016/j.cjche.2022.05.020.

Nomenclature

A	gas–liquid interfacial area, m^{-1}
a_A	amount of substance A, mol
C_O^*	initial oxygen concentration, %
C_O	dynamic oxygen concentration, %
c	concentration, $mol \cdot L^{-1}$
D_A	diffusion coefficient, $m \cdot s^{-1}$
d_b	bubble diameter, mm
$E(t)$	residence time distribution density function
$F(t)$	residence time distribution function
h_l	liquid level before oxygen bubbled, mm
h_{l+g}	liquid level after oxygen bubbled, mm
k	reaction rate constant, min^{-1}
$k_{A\text{-}B}$	reaction rate constant of A in B, min^{-1}
k_La	liquid-film mass transfer coefficient, min^{-1}
K_L	mass transfer coefficient in per unit interfacial area, $m \cdot min^{-1}$
M	mean molar mass, $g \cdot mol^{-1}$
$M_{l,s}$	phase interaction force, $N \cdot m^{-2}$
m_∞	total mass, mg
N_O	O_2 amount cross liquid film, $mmol \cdot min^{-1}$
p	pressure, $N \cdot m^{-2}$
T	temperature, °C or K
t	reaction time, s or min
u_g	gas velocity, $m \cdot s^{-1}$
u_l	liquid velocity, $m \cdot s^{-1}$
V	working volume of MMC, ml
V_A	gas molecular volume, $cm^3 \cdot mol^{-1}$
v_1	inlet liquid flow, $ml \cdot min^{-1}$
v_2	outlet liquid flow, $ml \cdot min^{-1}$
x_t	conversion, %
α_g	gas volume fraction
α_l	liquid volume fraction
γ	Hatta number
ε	gas holdup, %
μ	surface tension, mPa·s
ρ_l	liquid phase density, $kg \cdot m^{-3}$
ρ_g	gas phase density, $kg \cdot m^{-3}$
σ_l	liquid phase viscosity, $N \cdot m^{-1}$

References

[1] C.P. Vinod, K. Wilson, A.F. Lee, Recent advances in the heterogeneously catalysed aerobic selective oxidation of alcohols, *J. Chem. Technol. Biotechnol.* 86 (2) (2011) 161–171.
[2] F. Xu, Oxidation of phenols, anilines, and benzenethiols by fungal laccases: Correlation between activity and redox potentials as well as halide inhibition, *Biochemistry* 35 (23) (1996) 7608–7614.
[3] V.V. Torbina, A.A. Vodyankin, S. Ten, G.V. Mamontov, M.A. Salaev, V.I. Sobolev, O.V. Vodyankina, Ag-based catalysts in heterogeneous selective oxidation of alcohols: A review, *Catalysts* 8 (10) (2018) 447.
[4] T. Mallat, A. Baiker, Oxidation of alcohols with molecular oxygen on solid catalysts, *Chem. Rev.* 104 (6) (2004) 3037–3058.
[5] Y. Zhang, X.J. Cui, F. Shi, Y.Q. Deng, Nano-gold catalysis in fine chemical synthesis, *Chem. Rev.* 112 (4) (2018) 2467–2505.
[6] M. Sankar, Q. He, R.V. Engel, M.A. Sainna, A.J. Logsdail, A. Roldan, D.J. Willock, N. Agarwal, C.J. Kiely, G.J. Hutchings, Role of the support in gold-containing nanoparticles as heterogeneous catalysts, *Chem. Rev.* 120 (8) (2020) 3890–3938.
[7] E. Groppo, A. Lazzarini, M. Carosso, A. Bugaev, M. Manzoli, R. Pellegrini, C. Lamberti, D. Banerjee, A. Longo, Dynamic behavior of Pd/P4VP catalyst during the aerobic oxidation of 2-propanol: Asimultaneous SAXS/XAS/MS operand study, *ACS Catal.* 8 (8) (2018) 6870–6881.
[8] P. Sarmah, B.K. Das, P. Phukan, Novel dicopper(II)-tetracarboxylates as catalysts for selective oxidation of benzyl alcohols with aqueous TBHP, *Catal. Commun.* 11 (10) (2010) 932–935.
[9] L.M.T. Frija, M.L. Kuznetsov, B.G.M. Rocha, L. Cabral, M.L.S. Cristiano, M.N. Kopylovich, A.J.L. Pombeiro, Organocatalyzed oxidation of benzyl alcohols by a tetrazole-amino-saccharin: A combined experimental and theoretical (DFT) study, *Mol. Catal.* 442 (2017) 57–65.
[10] J. Zhao, Y.F. Zhang, L. Xu, F.P. Tian, T. Hu, C.G. Meng, Weak base favoring the synthesis of highly ordered V-MCM-41 with well-dispersed vanadium and the catalytic performances on selective oxidation of benzyl alcohol, *Chin. J. Chem. Eng.* 28 (5) (2020) 1424–1435.
[11] H. Gumus, Performance investigation of Fe_3O_4 blended poly (vinylidene fluoride) membrane on filtration and benzyl alcohol oxidation: Evaluation of sufficiency for catalytic reactors, *Chin. J. Chem. Eng.* 27 (2) (2019) 314–321.
[12] R.B. Cang, B. Lu, X.P. Li, R. Niu, J.X. Zhao, Q.H. Cai, Iron-chloride ionic liquid immobilized on SBA-15 for solvent-free oxidation of benzyl alcohol to benzaldehyde with H_2O_2, *Chem. Eng. Sci.* 137 (2015) 268–275.
[13] G.D. Yadav, M.S. Krishnan, Solid acid catalysed acylation of 2-methoxy-naphthalene: Role of intraparticle diffusional resistance, *Chem. Eng. Sci.* 54 (19) (1999) 4189–4197.
[14] S.R. Joshi, K.L. Kataria, S.B. Sawant, J.B. Joshi, Kinetics of oxidation of benzyl alcohol with dilute nitric acid, *Ind. Eng. Chem. Res.* 44 (2) (2005) 325–333.
[15] I.D. Somma, D. Russo, R. Andreozzi, R. Marotta, S. Guido, Kinetic modelling of benzyl alcohol selective oxidation in aqueous mixtures of nitric and sulfuric acids, *Chem. Eng. J.* 308 (2017) 738–744.
[16] K. Cerdan, W.Y. Ouyang, J.C. Colmenares, M.J. Muñoz-Batista, R. Luque, A.M. Balu, Facile mechanochemical modification of g-C_3N_4 for selective photo-oxidation of benzyl alcohol, *Chem. Eng. Sci.* 194 (2019) 78–84.
[17] H.B. Ji, K. Ebitani, T. Mizugaki, K. Kaneda, Oxidation of benzyl alcohol aiming at a greener reaction, *React. Kinet. Catal. Lett.* 78 (1) (2003) 73–80.
[18] G.Q. Liu, C.J. Zhao, G.Z. Wang, Y.X. Zhang, H.M. Zhang, Efficiently electrocatalytic oxidation of benzyl alcohol for energy-saved zinc-air battery using a multifunctional nickel-cobalt alloy electrocatalyst, *J. Colloid Interface Sci.* 532 (2018) 37–46.
[19] H. Li, F. Qin, Z.P. Yang, X.M. Cui, J.F. Wang, L.Z. Zhang, New reaction pathway induced by plasmon for selective benzyl alcohol oxidation on BiOCl possessing oxygen vacancies, *J. Am. Chem. Soc.* 139 (9) (2017) 3513–3521.
[20] D. Eisenberg, T.K. Slot, G. Rothenberg, Understanding oxygen activation on metal- and nitrogen-codoped carbon catalysts, *ACS Catal.* 8 (9) (2018) 8618–8629.
[21] I.M. Denekamp, M. Antens, T.K. Slot, G. Rothenberg, Selective catalytic oxidation of cyclohexene with molecular oxygen: Radical versus nonradical pathways, *ChemCatChem* 10 (5) (2018) 1035–1041.
[22] Y.H. Li, D. Nakashima, Y. Ichihashi, S. Nishiyama, S. Tsuruya, Promotion effect of alkali metal added to impregnated cobalt catalysts in the gas-phase catalytic oxidation of benzyl alcohol, *Ind. Eng. Chem. Res.* 43 (19) (2004) 6021–6026.
[23] Q. Wang, L.F. Chen, S.L. Guan, X. Zhang, B. Wang, X.Z. Cao, Z. Yu, Y.F. He, D.G. Evans, J.T. Feng, D.Q. Li, Ultrathin and vacancy-rich CoAl-layered double hydroxide/graphite oxide catalysts: promotional effect of cobalt vacancies and oxygen vacancies in alcohol oxidation, *ACS Catal.* 8 (4) (2018) 3104–3115.
[24] Y.T. Meng, H.C. Genuino, C.H. Kuo, H. Huang, S.Y. Chen, L.C. Zhang, A. Rossi, S.L. Suib, One-step hydrothermal synthesis of manganese-containing MFI-type zeolite, Mn-ZSM-5, characterization, and catalytic oxidation of hydrocarbons, *J. Am. Chem. Soc.* 135 (23) (2013) 8594–8605.
[25] Y. Fu, Y.L. Guo, Y. Guo, Y.S. Wang, L. Wang, W.C. Zhan, G.Z. Lu, *In situ* assembly of ultrafine Mn_3O_4 nanoparticles into MIL-101 for selective aerobic oxidation, *Catal. Sci. Technol.* 7 (18) (2017) 4136–4144.

[26] Y.H. Kim, S.K. Hwang, J.W. Kim, Y.S. Lee, Zirconia-supported ruthenium catalyst for efficient aerobic oxidation of alcohols to aldehydes, *Ind. Eng. Chem. Res.* 53 (31) (2014) 12548–12552.
[27] H.B. Ji, Q.L. Yuan, X.T. Zhou, L.X. Pei, L.F. Wang, Highly efficient selective oxidation of alcohols to carbonyl compounds catalyzed by ruthenium (III) meso-tetraphenylporphyrin chloride in the presence of molecular oxygen, *Bioorg. Med. Chem. Lett.* 17 (22) (2007) 6364–6368.
[28] Q. Han, X.X. Guo, X.T. Zhou, H.B. Ji, Efficient selective oxidation of alcohols to carbonyl compounds catalyzed by Ru-terpyridine complexes with molecular oxygen, *Inorg. Chem. Commun.* 112 (2020) 107544.
[29] C.H. Liu, C.Y. Lin, J.L. Chen, K.T. Lu, J.F. Lee, J.M. Chen, SBA-15-supported Pd catalysts: The effect of pretreatment conditions on particle size and its application to benzyl alcohol oxidation, *J. Catal.* 350 (2017) 21–29.
[30] J. Kobayashi, Y. Mori, S. Kobayashi, Multiphase organic synthesis in microchannel reactors, *Chem. Asian J.* 1 (1–2) (2006) 22–35.
[31] A.Y. Olenin, P.G. Mingalev, G.V. Lisichkin, Partial catalytic oxidation of alcohols: Catalysts based on metals and metal coordination compounds (a review), *Pet. Chem.* 58 (8) (2018) 577–592.
[32] Y. Ide, S. Tominaka, H. Kono, R. Ram, A. Machida, N. Tsunoji, Zeolitic Intralayer microchannels of magadiite, a natural layered silicate, to boost green organic synthesis, *Chem. Sci.* 9 (46) (2018) 8637–8643.
[33] S.N. Zhao, C.Q. Yao, Z.Y. Dong, Y.Y. Liu, G.W. Chen, Q. Yuan, Intensification of liquid-liquid two-phase mass transfer by oscillating bubbles in ultrasonic microreactor, *Chem. Eng. Sci.* 186 (2018) 122–134.
[34] G.W. Wu, A. Constantinou, E.H. Cao, S. Kuhn, M. Morad, M. Sankar, D. Bethell, G.J. Hutchings, A. Gavriilidis, Continuous heterogeneously catalyzed oxidation of benzyl alcohol using a tube-in-tube membrane microreactor, *Ind. Eng. Chem. Res.* 54 (16) (2015) 4183–4189.
[35] X. Zhang, H. Liu, A. Samb, G.F. Wang, CFD simulation of homogeneous reaction characteristics of dehydration of fructose to HMF in micro-channel reactors, *Chin. J. Chem. Eng.* 26 (6) (2018) 1340–1349.
[36] Y.P. Hu, C. Dong, T. Wang, G.S. Luo, Cyclohexanone ammoximation over TS-1 catalyst without organic solvent in a microreaction system, *Chem. Eng. Sci.* 187 (2018) 60–66.
[37] N.H. Othman, Z.T. Wu, K. Li, Micro-structured $Bi_{1.5}Y_{0.3}Sm_{0.2}O_{3-\delta}$ catalysts for oxidative coupling of methane, *AIChE J.* 61 (10) (2015) 3451–3458.
[38] K. Bawornruttanaboonya, S. Devahastin, A.S. Mujumdar, N.A. Laosiripojana, Computational fluid dynamic evaluation of a new microreactor design for catalytic partial oxidation of methane, *Int. J. Heat Mass Transf.* 115 (2017) 174–185.
[39] Y.M. Bruschi, E. López, M.N. Pedernera, D.O. Borio, Coupling exothermic and endothermic reactions in an ethanol microreformer for H_2 production, *Chem. Eng. J.* 294 (2016) 97–104.
[40] T. Jiwanuruk, S. Putivisutisak, P. Ponpesh, P. Bumroongsakulsawat, T. Tagawa, H. Yamada, S. Assabumrungrat, Effect of flow arrangement on micro membrane reforming for H_2 production from methane, *Chem. Eng. J.* 293 (2016) 319–326.
[41] N. Kockmann, D.M. Roberge, Harsh reaction conditions in continuous-flow microreactors for pharmaceutical production, *Chem. Eng. Technol.* 32 (11) (2009) 1682–1694.
[42] E. Kertalli, J.C. Schouten, T.A. Nijhuis, Direct synthesis of propylene oxide in the liquid phase under mild conditions, *Appl. Catal. A Gen.* 524 (2016) 200–205.
[43] F. Mashhadi, A. Habibi, K. Varmira, Enzymatic production of green epoxides from fatty acids present in soapstock in a microchannel bioreactor, *Ind. Crops Prod.* 113 (2018) 324–334.
[44] W. Wu, G. Qian, X.G. Zhou, W.K. Yuan, Peroxidization of methyl ethyl ketone in a microchannel reactor, *Chem. Eng. Sci.* 62 (18–20) (2007) 5127–5132.
[45] Q. Han, X.T. Zhou, X.Q. He, H.B. Ji, Mechanism and kinetics of the aerobic oxidation of benzyl alcohol to benzaldehyde catalyzed by cobalt porphyrin in a membrane microchannel reactor, *Chem. Eng. Sci.* 245 (2021) 116847.
[46] S.C. Galbraith, S. Park, Z. Huang, H. Liu, R.F. Meyer, M. Metzger, M.H. Flamm, S. Hurley, S. Yoon, Linking process variables to residence time distribution in a hybrid flowsheet model for continuous direct compression, *Chem. Eng. Res. Des.* 153 (2020) 85–95.
[47] J.D. Babbitt, Note on the fundamental law of diffusion, *J. Chem. Phys.* 23 (3) (1955) 601–602.
[48] P. Painmanakul, K. Loubière, G. Hébrard, M. Mietton-Peuchotb, M. Roustana, Effect of surfactants on liquid-side mass transfer coefficients, *Chem. Eng. Sci.* 60 (22) (2005) 6480–6491.
[49] K.R. Westerterp, L.L. van Dierendonck, J.A. de Kraa, Interfacial areas in agitated gas-liquid contactors, *Chem. Eng. Sci.* 18 (3) (1963) 157–176.
[50] F. Yoshida, Y. Miura, Gas absorption in agitated gas-liquid contactors, *Ind. Eng. Chem. Proc. Des. Dev.* 2 (4) (1963) 263–268.
[51] W.T. Koetsier, D. Thoenes, Mass Transfer in a closed stirred gas/liquid contactor: part 2: The liquid phase mass transfer coefficient kl, *Chem. Eng. J.* 5 (1) (1973) 71–75.
[52] O. Chedeville, M. Debacq, C. Porte, Removal of phenolic compounds present in olive mill wastewaters by ozonation, *Desalination* 249 (2) (2009) 865–869.
[53] Y. Haroun, D. Legendre, L. Raynal, Direct numerical simulation of reactive absorption in gas-liquid flow on structured packing using interface capturing method, *Chem. Eng. Sci.* 65 (1) (2010) 351–356.
[54] K. Sundmacher, L.K. Rihko, U. Hoffmann, Classification of reactive distillation processes by dimensionless numbers, *Chem. Eng. Commun.* 127 (1) (1994) 151–167.
[55] K. Hayashi, A. Tomiyama, Effects of surfactant on terminal velocity of a Taylor bubble in a vertical pipe, *Int. J. Multiph. Flow* 39 (2012) 78–87.